A Numerical Approach for the Design of Anode Beam Mechanical Systems

Andre Felipe Schneider, Olivier Charette and Daniel Richard

Hatch, 5 Place Ville-Marie, Suite 1400, Montréal, Québec, Canada, H3B 2G2

Keywords: Anode Jacking System, Anode Beam Lifting Mechanism, Mechanical Design, Finite Element Analysis

Abstract

Anode beam mechanical systems play an active role in the operation of modern aluminum reduction cells by enabling the anode bridge vertical displacement, and consequently, control of the anode-cathode distance. At the most basic level, however, they transfer motion from actuators to the anode beam while transmitting anode panel loads to the superstructure's fixed beam.

Said loads depend not only on the mass of both suspended anodes and crust but also on operational procedures: while the total suspended weight varies from startup to steady-state operation, weight distribution varies throughout the anode cycle. Different anode setting patterns yield different load distributions and significant dynamic loads arise from beam movements.

An approach for the analysis and design of anode beam mechanical systems was developed using ANSYS™-based numerical simulation and *in situ* measurements. A test case is presented and the impact of increased anode weight, selected operational procedures and design details is discussed.

Introduction

With amperage creep, anode weight is often increased such that anode beam mechanical systems are subjected to increasing loads. In practice, quantification of these loads is not straightforward. The total suspended weight varies from start-up, usually with a set of full size anodes, minimal anode cover and low anode immersion in bath, to steady-state operations, with partially consumed anodes, full anode cover and the counter-acting Archimedes forces (buoyancy). Moreover, weight is not uniformly distributed on the anode beam due to the anode cycle and setting patterns that will yield different load distributions. Finally, significant dynamic loads arise from beam movements.

This article introduces a methodology to assess the behavior of anode bridge mechanical systems based on numerical analysis and *in* situ measurements.

Anode Bridge Mechanical Systems

While some reduction technologies are capable of displacing individual anode pairs, most focus on overall anode-cathode distance (ACD) control by means of uniform anode bridge vertical motion. The latter is based on the synchronous motion of all anode bridge holding points, which can be achieved by different means, for instance activating several jacks simultaneously or using the parallelogram linkage. This classical four-bar mechanism – see Figure 1 – grants parallel motion between its opposite members and has been used as a template for the design anode bridge lifting mechanisms of several different technologies [1, 2, 3].

a) Parallelogram linkage[1]: (s + l = p + q)
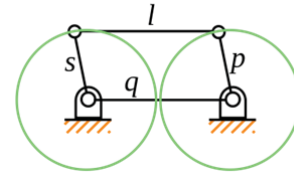
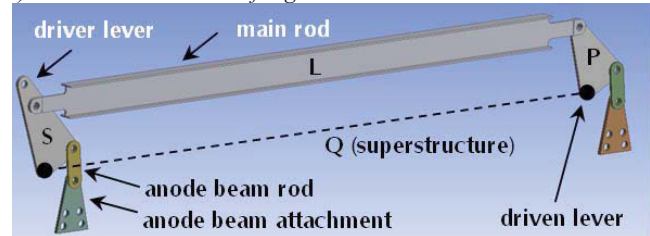*b) Generic anode beam lifting mechanism*

Figure 1 – The classical parallelogram linkage (a) can be used for the design of anode bridge lifting mechanisms (b).

Loads Acting on Anode Bridge Mechanical Systems

The loads acting on anode bridge mechanical systems are:

- Anode bridge's own mass (constant);
- Total anode panel load (including yokes, stems, cast iron and attachments to the anode bridge): decreases from startup to steady-state operation, as per Figure 2.
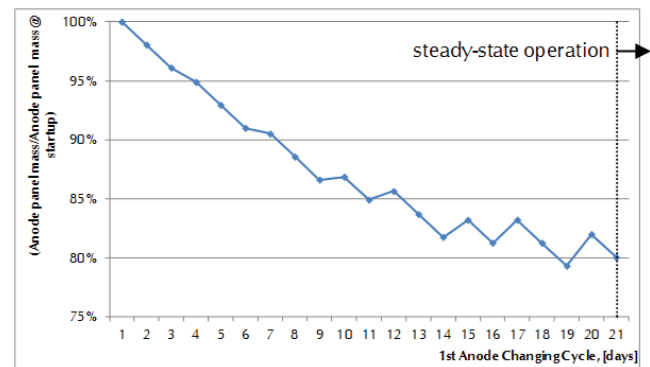

Figure 2 – Example of the evolution of the total anode panel load (buoyancy and crust mass excluded) from startup to the end of the 1st anode changing cycle.

- Spatial distribution of anode loads: varies with the anode changing cycle, as can be seen in Figure 3. The mass of each individual anode assembly can be obtained from Equation (1):

---

[1] Reproduced from http://en.wikipedia.org/wiki/Four-bar_linkage.

$$m_{assemb} = \left[m_{an0} - \left(c_{day} \cdot n_{service} \right) \right] + \left(m_{rod} + m_{yoke} + m_{iron} + m_{attach} \right) \qquad (1)$$

Where: m_{assemb} is the mass of the anode assembly, [kg]; m_{an0} is the mass of the new (baked) anode, [kg]; c_{day} is the anode consumption rate, [kg/day]; $n_{service}$ is anode service time, [days]; m_{rod} is the anode rod mass, [kg]; m_{yoke} is the yoke mass, [kg]; m_{iron} is the cast iron mass, [kg]; and m_{attach} is the mass of the attachment device (J-hooks and connectors), [kg].
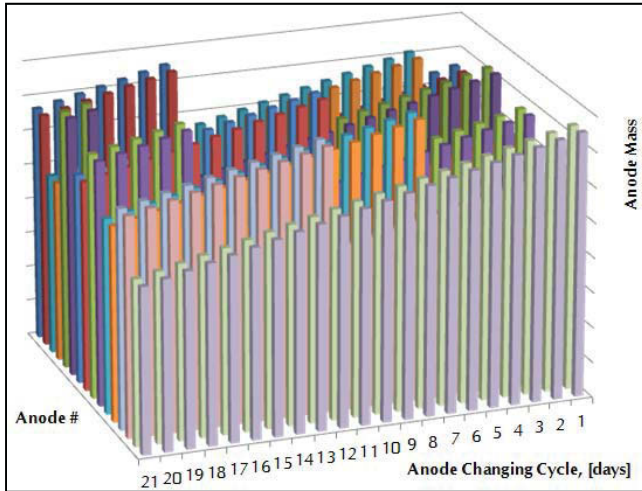

Figure 3 – Example of the spatial distribution of the anode load variation during the anode changing cycle.

Note that said uneven mass distribution may lead to non-uniform loading of the anode bridge mechanical system's components. Consider the ideal case of a simply supported beam subjected to a concentrated load W, as per Figure 4: the reactions R_1 and R_2 are a function of the positioning of W with respect to both supports, as per Equation (2).
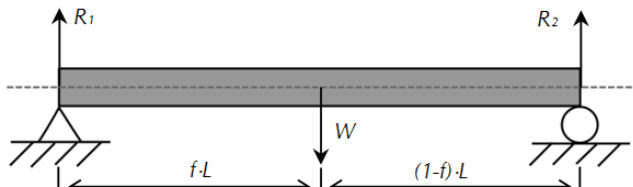

Figure 4 – The simply supported beam problem.

$$R_1 = (1 - f) \cdot W$$
$$R_2 = (f) \cdot W \qquad (2)$$

Where: L is distance between supports, [m]; W is the concentrated load, [N]; R_1 and R_2 are the reactions, [N]; and $0 \leq f \leq 1$.

This result indicates that different anode changing patterns leading to different spatial load distributions may yield different responses from the lifting mechanism.

- Anode buoyancy: as soon as the liquid phases are added to the cell, the apparent mass of the anode assembly is reduced due to buoyancy, as per Equation (3).

$$m_{red,buoyancy} = -\rho_{bath} \cdot \left(l_{an} \cdot w_{an} \cdot h_{im} \right) \qquad (3)$$

Where: $m_{red,buoyancy}$ is the apparent reduction of the anode assembly's mass due to buoyancy, [kg]; ρ_{bath} is the bath density, [kg/m³]; l_{an} is the anode length, [m]; w_{an} is the anode width, [m]; and h_{im} is the anode immersed height, [m].

- Anode cover: as soon as crust is formed and anodes are covered, the apparent mass of each anode assembly is increased according to Equation (4).

$$m_{inc,crust} = \left[\left(\rho_{solid} \cdot h_{solid} \right) + \left(\rho_{loose} \cdot h_{loose} \right) \right] \cdot \left(w_{cavity} \cdot l_{cavity} \right) \qquad \textbf{(4)}$$

Where: $m_{inc,crust}$ is the apparent increase of the anode assembly's mass due to cover, [kg]; ρ_{solid} is the density of the solid part of the anode cover, [kg/m³]; h_{solid} is the height of the solid part of the anode cover, [m]; ρ_{loose} is the density of the loose part of the anode cover, [kg/m³]; h_{loose} is the height of the loose part of the anode cover, [m]; w_{cavity} is the total width of the cavity (including 2 lengths of anodes, 2 lateral channels and one central channel), [m]; and l_{cavity} is the total length of the cavity (including (n_{an}/2) anodes widths, [(n_{an}/2)-1] inter-anode channels, and 2 end channels), [m]. Note that n_{an} is the total number of anodes. Furthermore, it is assumed that the composition and heights of anode covering material are similar between channels and above anodes.

Finally, it is obvious that an increase in potline current is likely to increase the total loading of the anode bridge lifting mechanism as anodes tend to be enlarged by the smelters in order to compensate for increased carbon consumption rate (c_{day}), often in an attempt to maintain work schedules.

Dynamic Loading

The static loads described above may be considerably increased by dynamic effects generated by anode beam movements, as evidenced by actual load measurements on a real-life anode bridge lifting mechanism under steady-state operation conditions (Figure 5). Note that the actual dynamic amplification factor for an existing technology can be obtained by monitoring its on-duty performance and comparing the obtained field data with the theoretical loads.
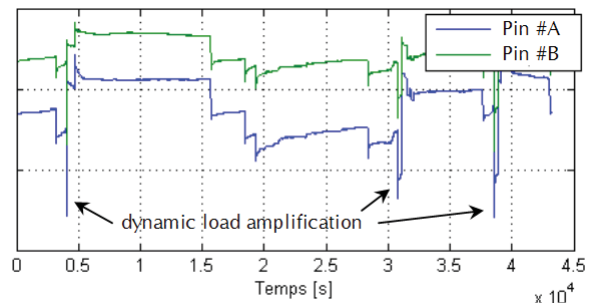

Figure 5 – Example of the dynamic load amplification due to anode beam movements.

Impact of Anode Beam Position and Dimensional Variations on Parallelogram Linkage-Type Anode Bridge Mechanical Systems

Anode bridges driven by mechanisms based on the classical parallelogram linkage have their vertical displacements coupled with a correspondent lateral movement due to the rotational nature

of the system. As a consequence, the loads acting on each one of its components vary with the anode beam vertical travel.

Furthermore, the nominal load distribution is based on the premise that each one of mechanism's opposite links have exactly the same length, *i.e.*, *l=q* and *s=p* (an ideal parallelogram, as per Figure 1). As real-life parts have fabrication and/or construction tolerances, variations in components dimensions may lead to loads distributions that differ from the theoretical values.

In order to assist smelters to evaluate the performances of anode bridge mechanical systems under realistic operating conditions, an assessment methodology based on numerical simulation and *in-situ* measurements was developed.

Approach Description

The overall behavior of an anode bridge lifting mechanism is obtained by means of a global one-dimensional (1D) finite-element (FE) model while the individual performance of each one of the system's components can be further assessed by means of detailed three-dimensional (3D) models. In order to validate and calibrate the numerical models, experimental data can be obtained by means of load cells installed onto existing mechanical systems.

Figure 6 shows the typical analyses involved in the assessment of anode bridge lifting mechanisms performance.
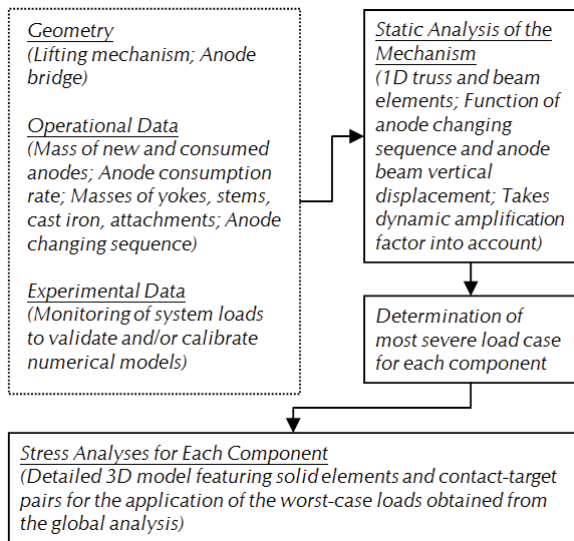

Figure 6 – Typical workflow for the assessment of anode bridge lifting mechanisms performance.

Global 1D Model

The overall behavior of the system is assessed by means of a global 1D model featuring the geometry of the mechanism itself as well as that of the anode bridge, both modeled by means of truss and beam elements – see Figure 7. The anode bridge-to-superstructure interaction is taken into account by means of compressive only truss elements with convenient degrees of freedom (DOF) coupled (CP) between their two defining nodes. This is necessary to avoid spurious traction and, consequently, unrealistic loss of contact.
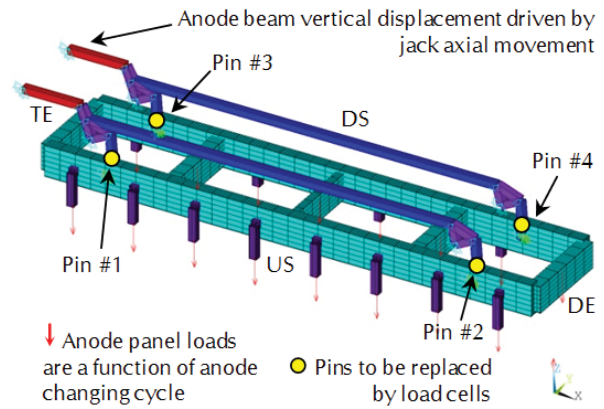

Figure 7 – Example of global 1D lifting mechanism model.

The response of the system is evaluated throughout the anode bridge travel for each day of the anode changing cycle. Anode beam vertical displacement is generated by the axial movement of the jacks.

Finally, dynamic amplification of the theoretical anode loads is taken into account and the worst load case for each components is determined.

Detailed 3D Models

Once the worst-case condition loads are obtained for each component, their individual response in terms of stresses and strains can be calculated by means of detailed 3D models – see Figure 8. The component's lateral displacement is limited by either blocking convenient DOF or by using a symmetry plane. In-plane movement is driven by contact-target pairs representing the pins-to-component interaction, which have the function of applying the loads obtained from the global 1D analysis.
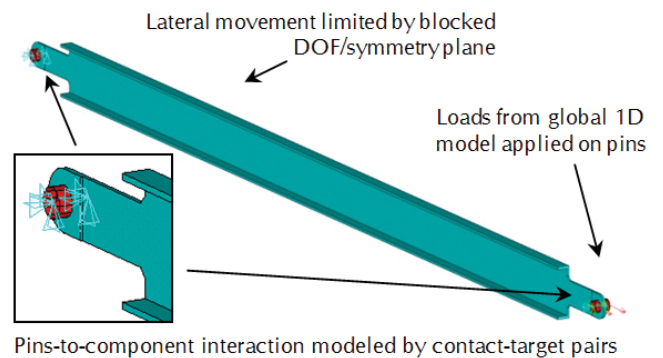

Figure 8 – Example of a detailed 3D model for the assessment of component stresses based on worst-case condition loads.

Test Case Model

In order to illustrate the capabilities of the proposed approach, a fictitious anode bridge mechanical system – previously shown in Figure 7 – will have its performance assessed. This equipment allows for a total anode bridge travel of 200 mm and is employed in a fictitious reduction technology previously introduced in [4] – see Figure 9.
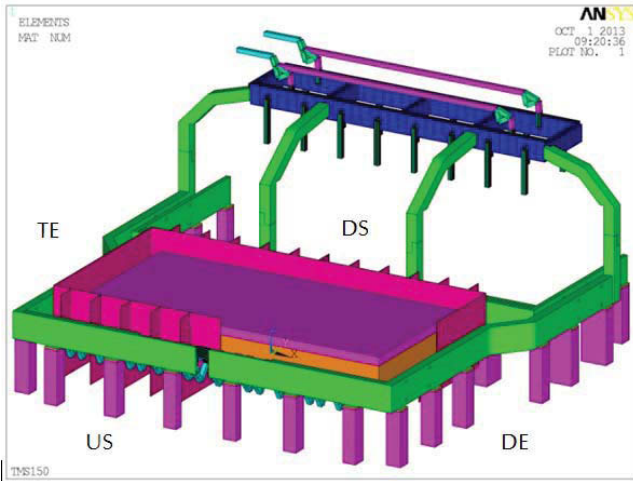
681

Figure 9 – Fictitious reduction technology.

These cells were originally designed for 150 kA, having 16 anodes of 1400 mm x 825 mm x 550 mm and were using a butterfly-type anode change pattern[2], shown in Figure 10. A series of modifications were introduced and enabled pot operation at 200 kA, including an anode size increase. Recently, with the aim of improving anode cover, a cascade-type anode changing pattern[3] (Figure 11) was put in service. Table 1 summarizes the data assumed for the analysis.

Table 1 – Operational data.

OPERATIONAL DATA	150	200	kA
Baked Carbon Block			
Length (overall)	1.4	1.6	m
Width (overall)	0.825	0.85	m
Height (overall)	0.55	0.6	m
Density	1550	1550	kg/m^3
Carbon Mass	912	1199	kg
Carbon Consumption			
Anode Changing Cycle Length	21	21	days
Carbon Consuption Rate	28.6	38.2	kg/day
Anode Butt Height	0.214	0.220	m
Other Anode Assembly Components			
Yoke, Stem, Cast Iron, Attachment	560	560	kg
Anode Assembly Mass at Startup (No Buoyancy or Anode Cover)			
New Anode Assembly	1472	1759	kg
Anode Buoyancy			
Immersed Depth	0.12	0.12	m
Bath Density	2113	2113	kg/m^3
Apparent Assembly Mass Reduction	-293	-345	kg
Anode Cover Mass			
Cavity Surface/Anode	1.631	1.631	m^2
Solid Cover Density	2600	2600	kg/m^3
Solid Cover Height	0.05	0.05	m
Solid Cover Mass/Anode	212	212	kg
Loose Cover Density	1800	1800	kg/m^3
Loose Cover Height	0.05	0.05	m
Loose Cover Mass/Anode	147	147	kg
Apparent Assembly Mass Increase	359	359	kg
Apparent Anode Assembly Mass at Steady-State Operation			
New Anode Assembly	1538	1773	kg
Anode Butt	965	1009	kg
Total Anode Bridge Mass			
Total Anode Bridge Mass	3700	3700	kg

[2] Adapted from "Rota A" anode changing pattern from [5].
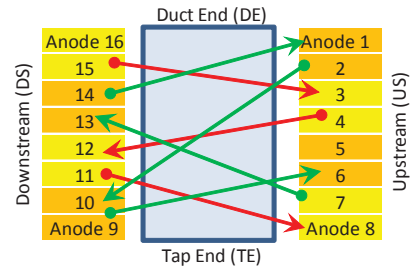[3] Adapted from "Rota B" anode changing pattern from [5].

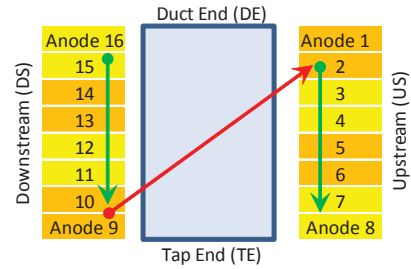**Figure 10 – Original "butterfly" anode change pattern.**

Figure 11 – New "cascade" anode change pattern.

In order to assess the system's mechanical performance under these new operational conditions, one anode bridge lifting mechanism was instrumented during pot relining, having its anode beam rod-to-attachment pins replaced by load cells – see Figure 7. Analysis of acquired data revealed a dynamic amplification factor $k_{dyn} = 1.5$, taken into account in all subsequent calculations. The main rods and anode beam rods (both identified in Figure 1) will be used in this paper to illustrate typical results obtained with the numerical models.
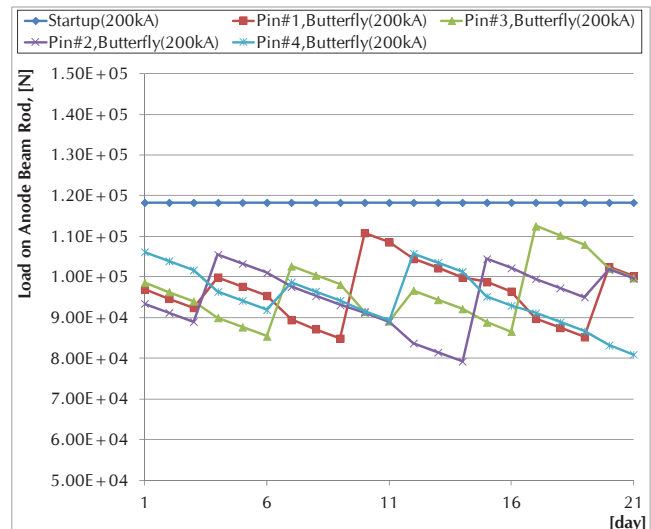
Anode Beam Rods Performance at 200 kA

Figure 12 – Load magnitudes for anode beam rods at 200 kA: startup and "butterfly" anode change cycle.

Figure 12 shows the magnitude of the loads acting on the anode beam rods[4] for both startup and steady-state operation at 200 kA (using 1600 mm long anodes) during an ideal startup (i.e., neither

[4] Pins are identified in the above-mentioned Figure 7.

cover nor buoyancy are considered) and throughout one full anode change cycle using the "butterfly" pattern. Note that all components are considered at their nominal dimensions.

The maximum forces on anode beam rods generated by the new cascade-type anode change pattern, however, are even larger than those obtained during startup, as per Figure 13. This change in philosophy does tend to concentrate the new heavier anodes under a single rod as the cycle goes on. Furthermore, the increase of the variation of the load magnitude throughout the "cascade" cycle when compared to the original "butterfly" pattern is remarkable.
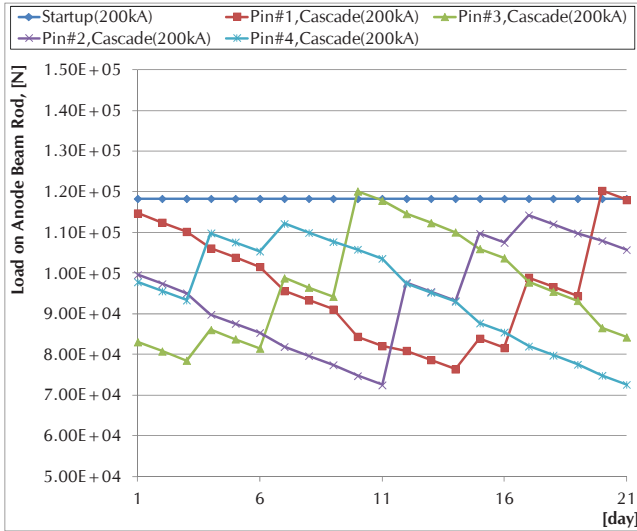

Figure 13 – Load magnitudes for anode beam rods at 200 kA: startup and "cascade" anode change cycle.

Figure 14 shows the comparison between measured and predicted loads acting on anode beam rods throughout one full "cascade" anode change cycle. Note that all components of this real-life anode bridge lifting mechanism are considered at their nominal dimensions. A fair agreement is observed between experimental and numerical data.
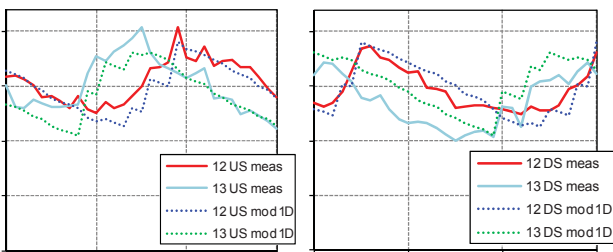

Figure 14 – Example of a comparison between measured and predicted loads on anode beam rods throughout one full "cascade" anode change cycle.

Finally, a sensitivity study regarding the impact of fabrication tolerances on the anode beam rod loads distribution was performed. Figure 15 shows the impact of modifying the dimensions of main rods (5250±1.0 mm) and anode beam rods (250±0.5 mm) within the specified tolerances (see Table 2): a substantial increase in both the maximum magnitude and variation of the anode beam rod loads can be seen when compared with Figure 13.

Table 2 – Dimensional variations considered for the sensitivity analysis, [mm].

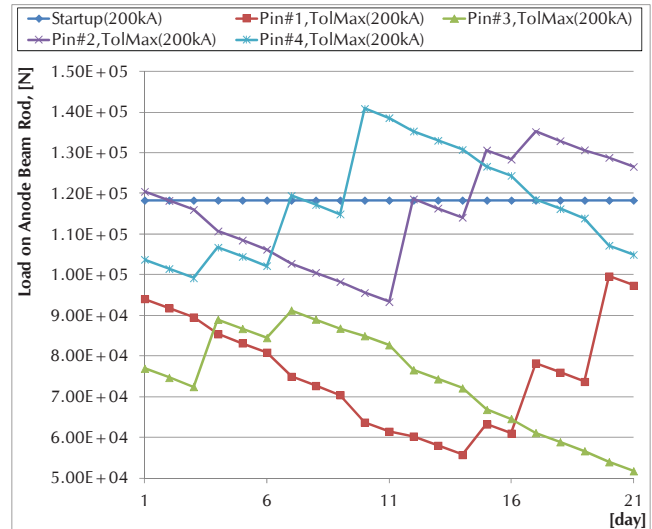|	
Anode beam rod (US/TE)	+0.5
Anode beam rod (DS/TE)	-0.5
Anode beam rod (US/DE)	-0.5
Anode beam rod (DS/DE)	+0.5
Main rod (US)	-1.0
Main rod (DS)	+1.0

Figure 15 – Load magnitudes for anode beam rods at 200 kA: startup and "cascade" anode change cycle including dimensional variations.

Figure 16 (a) shows the comparison between measured and predicted loads acting on anode beam rods throughout one full "cascade" anode change cycle for a bridge jacking mechanism similar to that previously studied on Figure 14. A considerable discrepancy between numerical predictions and experimental data was observed when using nominal geometry.

a) Nominal dimensions
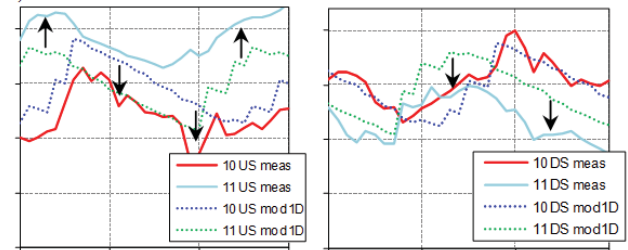
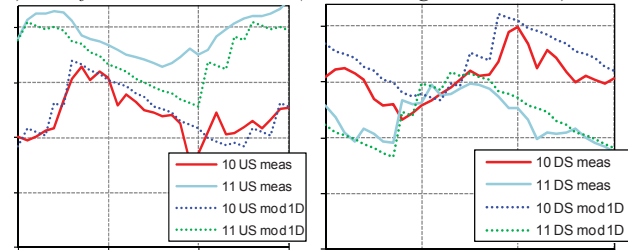*b) Modified anode beam rods (nominal length ±0.375mm)*

Figure 16 – Comparison between measured and predicted loads on anode beam rods throughout one full "cascade" anode change cycle considering (a) nominal dimensions and (b) modified anode beam rods.

This rather odd behavior led to the investigation of the potential impact of modifying the distance between the 2 pins of the anode rods by ±0.375 mm on the system's load distribution. The outcome of said analysis is the fair agreement observed between numerical and experimental anode beam rod loads shown in Figure 16 (b). This highlights the importance of considering fabrication tolerances when performing these analyses.

Table 3 shows that the minimum safety factor with respect to yield (SF_Y) is larger than unity in all cases when considering nominal dimensions. However, the results show that plastic deformation is possible in normal operation with the cascade anode setting pattern when considering variation of components geometry within the fabrication tolerances. The typical SF_Y distribution for these components can be seen in Figure 17.

Table 3 – Minimum SF_Y, [-], for anode beam rods at 200 kA and nominal dimensions.

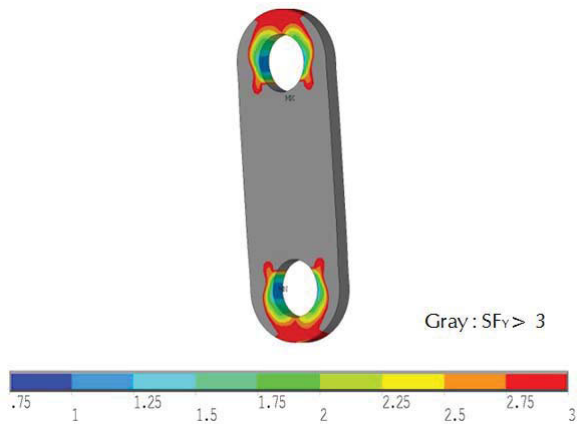| Case	Geometry	SF_Y, min
Startup	Nominal	1.07
Operation, Butterfly	Nominal	1.13
Operation, Cascade	Nominal	1.05
Operation, Cascade	As per Table 2	0.90

Gray : $SF_Y > 3$

Figure 17 – SF_Y, [-], for anode beam rods at 200 kA: startup.

Main Rods Performance at 200 kA

The analysis indicates that the main rods would experience plastic deformation (minimum SF_Y = 0.96) when starting up the cells at 200 kA (1600 mm long anodes), Figure 18. Note that all components are considered at their nominal dimensions. This shows that different components have different limiting cases.
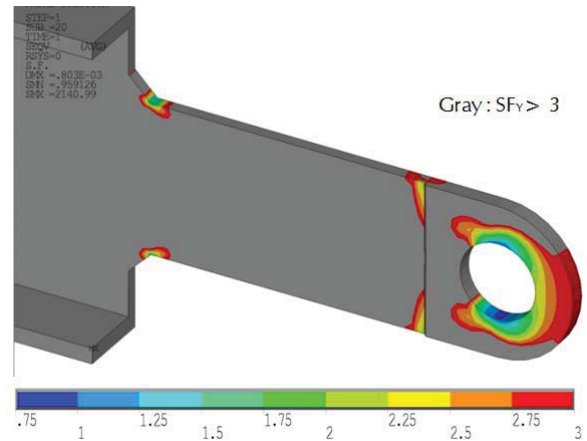

Gray : $SF_Y > 3$

Figure 18 – SF_Y, [-], for main rods (symmetric model) at 200 kA: startup.

Conclusions

An approach for the analysis and design of anode beam mechanical systems was developed using ANSYS™-based numerical simulation and *in situ* measurements. Evidence was shown that loads acting on different components of anode bridge mechanical systems are influenced not only by the masses of suspended anode assemblies but also by anode change patterns and the dimensional variations arising from fabrication tolerances. It is important to stress that the potential impact of the above-mentioned features should not be ignored when either designing or assessing the mechanical performance of this kind of equipment.

References

[1] Lu Dingxiong, Ban Yungang, Qin Junman and Ai Zijin, "New Progress on Application of NEUI400kA Family High Energy Efficiency Aluminum Reduction Pot ("HEEP") Technology", Proc. Light Metals 2011, TMS, Warrendale, PA, pp. 443-448.
[2] Kangjian Sun, Hongwu Hu, Jiaming Zhu, Xiaodong Yang, and Jun Chen, "The Newly Advancement of SY400 Pot", Proc. Light Metals 2010, TMS, Warrendale, PA, pp. 355-357.
[3] Alton Taberaux, "Prebake Cell Technology: A Global Review", JOM Volume 52, Number 2 (February 2000), TMS, Warrendale, PA, pp. 22-29.
[4] A.F. Schneider, D. Richard and O. Charette, "Impact of Amperage Creep on Busbars and Electrical Insulation: Thermal-Electrical Aspects", Proc. Light Metals 2011, TMS, Warrendale, PA, pp 525-530.
[5] M. Iffert, M. Skyllas-Kazacos and B. Welch, "Challenges in Mass Balance Control", Proc. Light Metals 2005, TMS, Warrendale, PA, pp. 385-391.